Supporting Information for "Asian Irrigation, African Rain: Remote Impacts of Irrigation"

Philipp de Vrese,[1] Stefan Hagemann,[1] Martin Claussen,[1,2]

[1]Max Planck Institute for Meteorology, Bundesstrasse 53, 20146 Hamburg, Germany.

[2]Center for Earth System Research and Sustainability, University of Hamburg, Bundesstrasse 55, 20146 Hamburg, Germany.

0094-8276/16/$5.00

Contents of this file

1. Text S1. Model Description
2. Text S2. Irrigation Scheme
3. Text S3. Internal Model Variability
4. Figure 1. Winds
5. Figure 2. Irrigation
6. Figure 3. Impact of irrigation on the upward moisture flux
7. Figure 4. Water vapor, cloud cover, precipitation and surface temperatures
8. Figure 5. Atmospheric water vapor in different irrigation scenarios

Introduction

This supporting material aims to give additional information on ECAHM and JSBACH, the model components used for this study (S1), to provide a more detailed account of the irrigation scheme implemented into JSBACH (S2) and to describe the measure for the model's internal variability (S3). Furthermore, it provides figures generated based on model output that help clarify certain aspects of the main text. Fig. 1 shows how the simulated low atmospheric winds compare to ERA-Interim reanalysis data [*Dee et al.*, 2011]. Fig. 2 gives the spatial and temporal extent of irrigation, Fig. 3 shows the upward moisture flux within the region of interest, Fig. 4 helps to relate the additional atmospheric water vapor to changes in cloud cover, precipitation and surface temperature and Fig. 5 shows in which region the additional atmospheric water vapor can be found for the different irrigation simulations.

Text S1. Model Description
In JSBACH spatial sub-grid scale heterogeneity of the land surface is represented by tiles which are used explicitly in the simulation of physical processes at and below the surface. The tiles constitute homogeneous subareas within the grid box that correspond to different plant functional types, of which each represents a group of different species aggregated based on their functional properties (exceptions are bare soil areas and glaciers). The tiles within one grid box interact exclusively via the horizontal mixing of vertical turbulent fluxes in the atmosphere. On and below the surface, a horizontal sub-grid scale flow of water and heat is not represented in the model, and the soil moisture and temperature in a given tile is independent of the other tiles. With respect to hydrology, in this study no vertical levels are distinguished below ground, and the soil is represented using a simple bucket scheme [*Düllmenil and Tondini*, 1992].

The surface fluxes are calculated using a bulk-exchange formulation that applies approximate analytical expressions similar to those proposed by *Louis* [1979] to determine the transfer coefficients. In this study, the VERTEX scheme [*de Vrese et al.*, 2016] is used to couple surface and atmosphere. The scheme is a flux aggregating scheme, based on the assumption that within the lowest model levels of the atmosphere, the vertical fluxes have not completely blended and the atmosphere is horizontally heterogeneous up to a given height. Thus, the scheme explicitly accounts for spatial heterogeneity within the lowest layers of the atmosphere and resolves the vertical turbulent mixing process with respect to the surface tiles. In ECHAM the vertical fluxes are modelled by a modified version of the turbulent kinetic energy scheme proposed by *Brinkop and Roeckner* [1995]. The turbulent viscosity and diffusivity are described by a function of the turbulent kinetic energy, the turbulent mixing length [*Blackadar*, 1962] and a stability function that depends on the moist Richardson number [*Mellor and Yamada*, 1982]. In the VERTEX scheme, the fluxes are calculated for each tile individually within the lowest three layers of the atmosphere. Here, the fluxes within the individual tiles are not treated independently of each other but are assumed to mix horizontally to a certain extent. Thus, the vertical flux from a given tile influences the states of all tiles on the adjacent levels.

The extent to which the vertical fluxes blend horizontally is determined based on the ratio of the height of a model level and the blending height. The latter can be estimated as a function of friction velocity, the horizontal windspeed and the characteristic length scale of the respective surface heterogeneity [*Mahrt*, 2000]. In this study the characteristic length scales required for the computation of the blending height were derived from the Global Land Cover Map 2009 [*Congalton et al.*, 2014]. For areas in which the dataset classified agricultural areas as rainfed even though these are equipped for irrigation, the characteristic length scales were determined based on the areas of rainfed crops, assuming that the areas are equipped for irrigation but not irrigated during the passing of the satellite.

Sub-grid scale circulations, i.e. advection between individual tiles, are not explicitly represented in the VERTEX scheme, although they are accounted for in the expressions used to determine the extent to which the vertical fluxes blend horizontally. On the model's grid scale, the advective transport is modelled using the flux-form semi-Lagrangian scheme, proposed by *Lin and Rood* [1996], as the extension of an Eulerian multidimensional flux-form scheme.

Text S2. Irrigation Scheme
For $\mathrm{IRR}_{\mathrm{min}}$, JSBACH was equipped with an irrigation scheme in which irrigation is simulated by maintaining the soil moisture in the tile representing irrigated crops close to the level at which potential transpiration is reached, i.e. 75 % of the field capacity. The water is added directly to the soil and the skin reservoir is not affected. Thus, the water is accessible only for an uptake via the roots and leads to an increase in transpiration but not directly to an increase in evaporation from the plants skin reservoir.

In the present setup of JSBACH, each tile comprises a vegetated and a non-vegetated fraction, whose extents vary depending on the current state of vegetation (note that the permanent bare soil fraction, i.e. the area that is uninhabitable to vegetation, has already been integrated into a dedicated tile). While the amount of water required for irrigation was calculated only for the vegetated fraction, it was applied to the entire tile. Hence, unless the tile is fully vegetated the soil moisture after irrigation was below 75 % of the field capacity. The soil moisture in the irrigated tile was increased at the beginning of each 20-minute time step. The amount of water added during irrigation $I^t_{cr\_I}$ in time step t and the soil moisture in the irrigated crop tile $w^{t,start}_{cr\_I}$ at the beginning of each time step were calculated using the water holding capacity of the soil w_{cap}, a coefficient representing the fraction of soil moisture required for transpiration to occur at the potential rate c_{pot_trans} (0.75), the soil moisture in the irrigated tile at the end of the previous time step $w^{t-1,end}_{cr\_I}$ and the vegetation ratio at the beginning of the time step $v^{t,start}_{cr\_I}$.

$$\begin{aligned} I^t_{cr\_I} &= (w_{cap} \cdot c_{pot\_trans} - w^{t-1,end}_{cr\_I}) \cdot v^{t,start}_{cr\_I}, \\ w^{t,start}_{cr\_I} &= w^{t-1,end}_{cr\_I} + I^t_{cr\_I}, \\ \text{for} & \\ w^{t-1,end}_{cr\_I} &< w_{cap} \cdot c_{pot\_trans}. \end{aligned} \quad (1)$$

As explained above, the soil moisture within the irrigated crop tile is below 75 % of the field capacity, unless the tile is fully vegetated. This means that, especially during the beginning of the growing season, the crops will not transpire at the potential rate. Additionally, there is no direct increase in evaporation from the skin reservoir and only in a small share of the irrigated grid boxes bare soil evaporation is increased. In the simple bucket scheme used, bare soil evaporation only occurs when the soil is almost fully saturated, which for most grid boxes is not the case when the soil moisture is at or below $\approx$ 75 % of the field capacity. This scheme likely underestimates the irrigation induced moisture flux as, especially in rice growing regions where soils are actually saturated for the largest part of the growing season, evaporation from the non-vegetated parts of the fields may have a strong contribution to the overall moisture flux.

To be able to include an increase in evaporation, the irrigated crop tile was split into an irrigated vegetated tile, which on annual average constitutes roughly 1 % of the land surface, and a potentially irrigated non-vegetated tile, which constitutes the remaining 1 %. To ensure that the simulations were based on an identical area vegetated by irrigated crops, the cover fraction of the (fully vegetated) irrigated crop tile $cf_{v\_cr\_I,max}$ was prescribed based on the cover fraction $cf_{cr\_I,min}$ and the vegetation ratio $v_{cr\_I,min}$ of the irrigated crop tile taken from $\mathrm{IRR}_{\mathrm{min}}$. :

$$\begin{aligned} cf_{v\_cr\_I,max} &= cf_{cr\_I,min} \cdot v_{cr\_I,min}, \\ v_{v\_cr\_I,max} &= 1.0\ . \end{aligned} \quad (2)$$

The cover fractions were determined based on 20-year monthly mean values and the cover fraction for a give time

step was calculated by linearly interpolating between the monthly means.

The aim of the scenario $\mathrm{IRR}_{\mathrm{max}}$ is to additionally account for evaporation from bare soil areas and from parts of the irrigation infrastructure such as reservoirs and channels. To estimate the cover fraction of the area in which irrigation would induce evaporation we assumed that the regional irrigation efficiency, i.e. the ratio of evapotranspiration from crops to the total amount of water abstracted for irrigation, is proportional to the ratio of vegetated irrigated area and the absolute irrigated area. Accordingly, irrigation was applied in the fully vegetated crop tile and also in an irrigated bare soil tile. The cover fraction of the irrigated bare soil tile $cf_{bs\_I,max}$ was calculated based on the fraction of the vegetated crop tile and the assumed irrigation efficiency of a given region e_{reg}, taken from *Döll and Siebert* [2002],

$$\begin{aligned} cf_{bs\_I,max} &= cf_{cr\_I,min} \cdot v_{cr\_I,min} \cdot (1/e_{reg} - 1), \\ &\text{for} \\ & cf_{cr\_I,min} \cdot v_{cr\_I,min} \cdot (1/e_{reg} - 1) < \\ & cf_{bare,min} + cf_{cr\_I,min} \cdot (1 - v_{cr\_I,min}), \end{aligned}$$

otherwise

$$\begin{aligned} cf_{bs\_I,max} &= cf_{bare,min} \\ &+ cf_{cr\_I,min} \cdot (1 - v_{cr\_I,min}). \end{aligned} \tag{3}$$

Furthermore, the target soil moisture in irrigated regions was set to the field capacity, to best represent inundated surfaces in rice growing regions. The amount of water applied to the non-vegetated fraction is calculated analogous to Eq. 1 but omitting the scaling with the vegetation ratio and using w_{cap} as target soil moisture.

$$I^t_{bs\_I} = w_{cap} - w^{t-1,end}_{bs\_I} \tag{4}$$

In many irrigated areas, such as most parts of India, the bare soil fraction is comparatively small. Here, $cf_{bs\_I,max}$ is limited by the available bare soil area, and the ratio of vegetated irrigated area and absolute irrigated area is much larger than the regional irrigation efficiency. However, this scenario represents an overestimation of the actual irrigation induced moisture flux. In reality losses through runoff and drainage, which do not induce additional evaporation, will contribute to the total amount of water abstracted for irrigation. Therefore, $\mathrm{IRR}_{\mathrm{min}}$ and $\mathrm{IRR}_{\mathrm{max}}$ should be taken as scenarios that give an upper and lower boundary to the range in which the impact of real-world irrigation lies.

Text S3. Internal Model Variability

To evaluate the robustness of the differences between two simulations we used a Student's t-test in combination with a comparison to the model's internal variability [*Hagemann et al.*, 2009]. The internal model variability, with respect to 20-year mean values, was taken as the maximum intra-ensemble spread of three 20-year, 5-member ensembles, simulated with ECHAM/JSBACH. Note that, in order to make the measure more reliable, we use a different measure for the spread than in the study of Hagemann et al. In this study, the spread for each model grid box is defined as the difference between the ensemble maximum and the ensemble minimum, whereas Hagemann et al. used the standard deviation of an ensemble. Within each ensemble, the model setup is identical but the simulations were started using slightly differing initial conditions. To account for possible changes in the model's internal variability due to changes in the model's structure or parametrizations, each of three ensembles was simulated using a different scheme for the land surface-atmosphere coupling. These were a parameter aggregation scheme, a simple flux aggregation scheme and the newly developed VERTEX scheme [*de Vrese et al.*, 2016].

References

Blackadar, A. K. (1962), The vertical distribution of wind and turbulent exchange in a neutral atmosphere, *J. Geophys. Res.*, *67*(8), 3095–3102.

Brinkop, S., and E. Roeckner (1995), Sensitivity of a general circulation model to parameterizations of cloud–turbulence interactions in the atmospheric boundary layer, *Tellus A*, *47*(2), 197–220.

Congalton, R., J. Gu, K. Yadav, P. Thenkabail, and M. Ozdogan (2014), Global land cover mapping: A review and uncertainty analysis, *Remote Sens.*, *6*(12), 12,070–12,093.

de Vrese, P., J.-P. Schulz, and S. Hagemann (2016), On the representation of heterogeneity in land-surface-atmosphere coupling, *Boundary-Layer Meteorol.*, in print.

Dee, D., S. Uppala, A. Simmons, P. Berrisford, P. Poli, S. Kobayashi, U. Andrae, M. Balmaseda, G. Balsamo, P. B. P. Bechtold, A. Beljaars, L. van de Berg, J. Bidlot, N. Bormann, C. Delsol, R. Dragani, M. F. A. Geera, L. Haimberger, S. Healy, H. Hersbach, E. Holm, L. Isaksen, P. Kallberg, M. Koehler, M. Matricardi, A. McNally, B. Monge-Sanz, J. Morcrette, B. Park, C. Peubey, P. de Rosnay, C. Tavolato, J. Thepaut, and F. Vitart (2011), The era-interim reanalysis: Configuration and performance of the data assimilation system, *QJR meteorol. Soc.*, *137*(656), 553–597.

Döll, P., and S. Siebert (2002), Global modeling of irrigation water requirements, *Water Resour. Res.*, *38*(4), 8–1.

Düllmenil, L., and E. Tondini (1992), A rainfall-runoff scheme for use in the hamburg climate model, *‚J.P. O'Kane (Ed.): Advances in Theoretical Hydrology, A Tribune to James Dooge,*, pp. 129–157.

Hagemann, S., H. Göttel, D. Jacob, P. Lorenz, and E. Roeckner (2009), Improved regional scale processes reflected in projected hydrological changes over large European catchments, *Clim. Dyn.*, *32*(6), 767–781.

Lin, S.-J., and R. B. Rood (1996), Multidimensional flux-form semi-lagrangian transport schemes, *Mon. Weather Rev.*, *124*(9), 2046–2070.

Louis, J.-F. (1979), A parametric model of vertical eddy fluxes in the atmosphere, *Boundary-Layer Meteorol.*, *17*(2), 187–202.

Mahrt, L. (2000), Surface heterogeneity and vertical structure of the boundary layer, *Boundary-Layer Meteorol.*, *96*(1-2), 33–62.

Mellor, G. L., and T. Yamada (1982), Development of a turbulence closure model for geophysical fluid problems, *Rev. Geophys.*, *20*(4), 851–875.

Corresponding author: Philipp de Vrese, Max Planck Institute for Meteorology, Bundesstrasse 53, 20146 Hamburg, Germany. (philipp.de-vrese@mpimet.mpg.de)

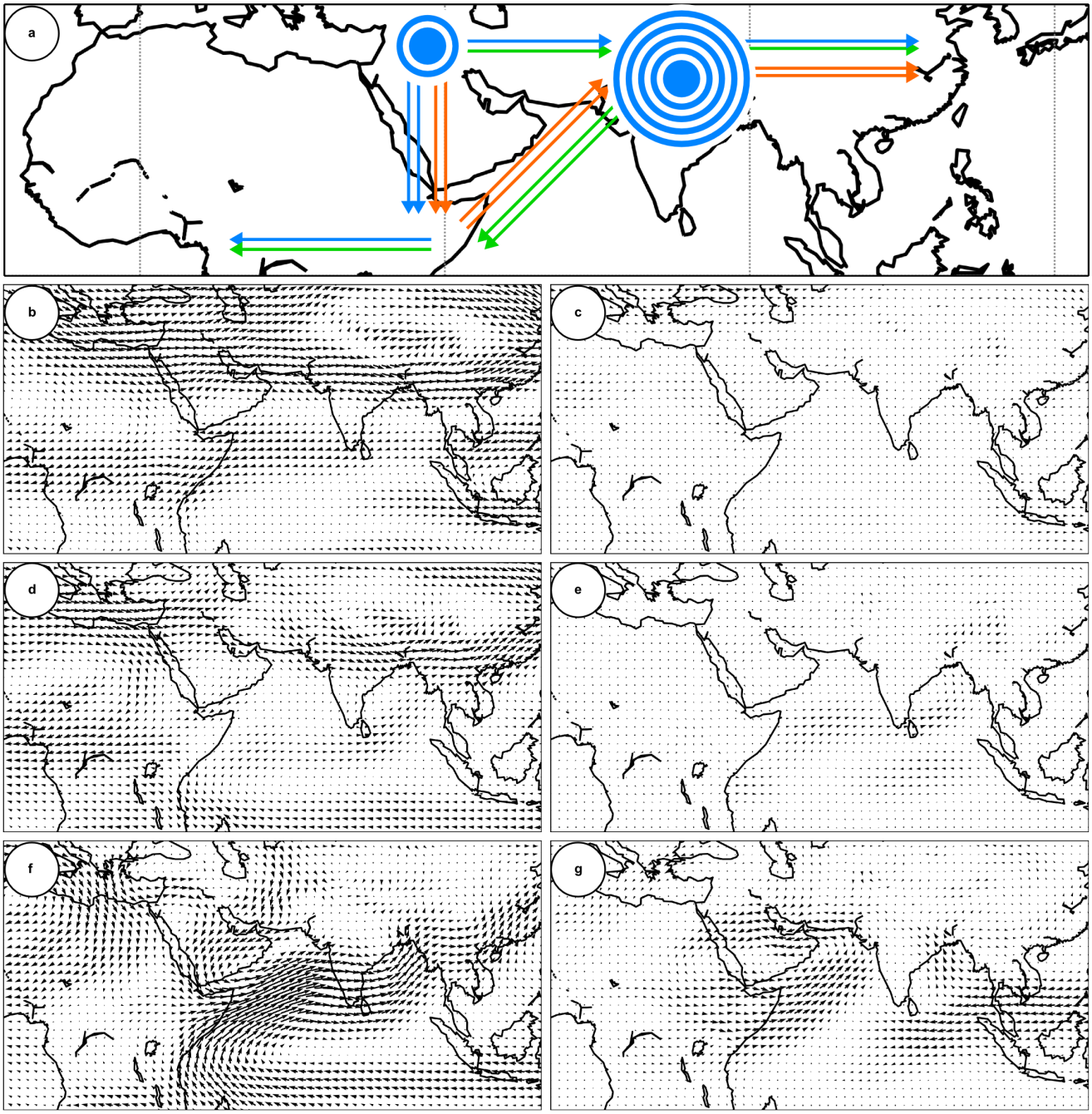

Supporting Material Fig. 1: Low atmospheric winds during spring and summer: a) Schematic (same as Fig. 2 a in the main text);
20-year mean winds simulated in IRRmin: b) February-March, d) April-May, f) June-July;
20-year mean differences between the winds in IRRmin and those obtained from reanalysis data: c) February-March, e) April-May, g) June-July

For early spring (February-March) the simulated low atmospheric winds (IRRmin) show a good agreement with ERA-Interim reanalyisis data [Dee et al., 2011]. In late spring (April-May) the agreement is still reasonable, even though it can allready be seen that the southwesterly winds in the Arabian Sea and the southerly winds in the Bay of Bangal are overestimated by the model. This is connected to the representation of the monsoon winds and the overstimation is even more pronouncd during the summer month (June-July). For these month, the model does not capture the related winds well. However, the simulations improve when irrigation is accounted for, even though the improvement is small compared to the overall bias.

This overstimation of southwesterly winds in the Arabian Sea also means that in reality the irigation-induced effects in Eastern Africa are possibly larger than in the simulations. It was argued that in summer, moisture from irrigated regions in the Middle East is transported towards the Horn of Africa, where it is advected eastwards by the southwesterly winds. If these winds are overstimated in the model, it is plausible that more water vapor remains in Eastern Africa and the related effects might still be perceivable during the summer month.

Figure S1.

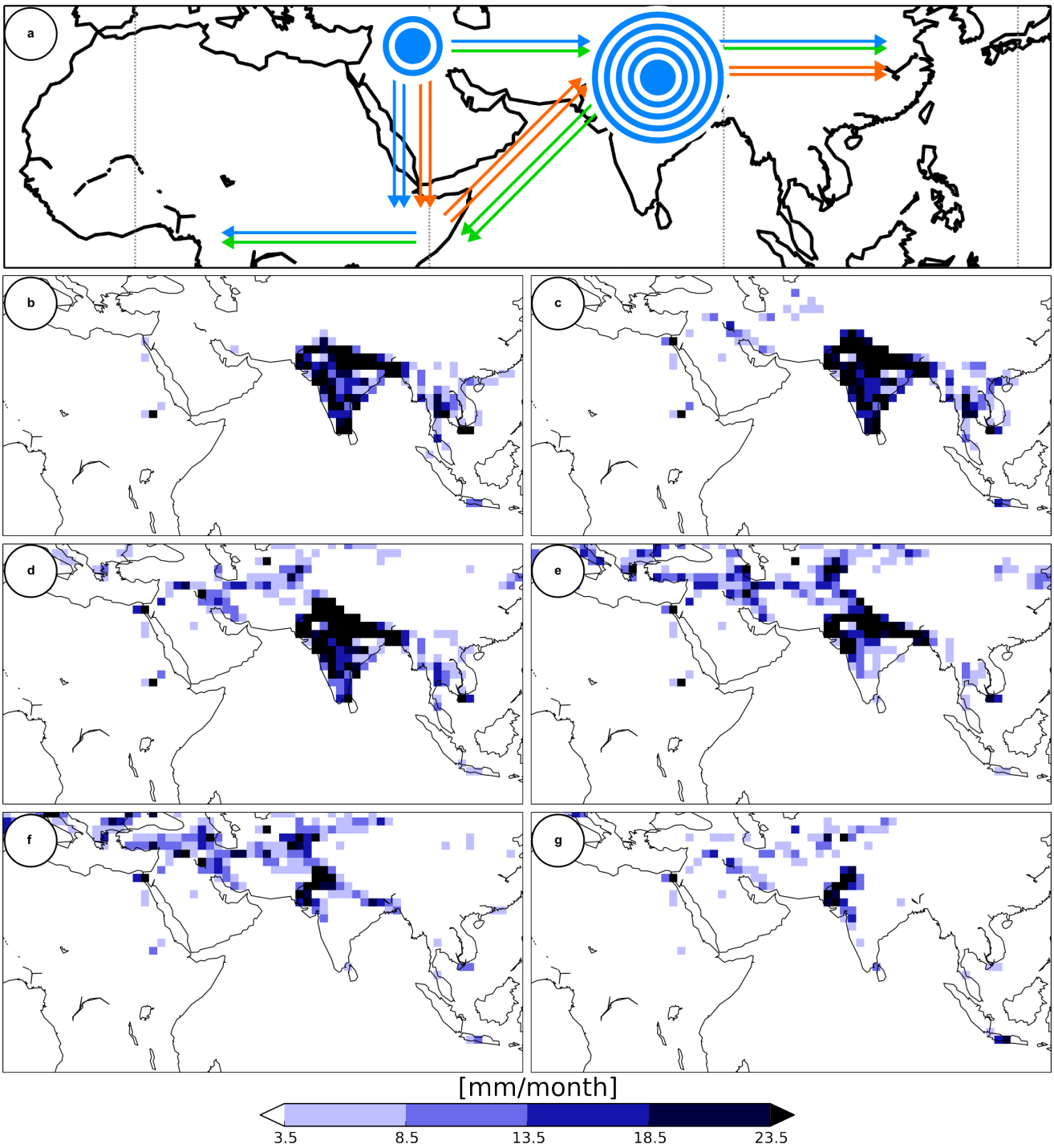

Supporting Material Fig. 2: Irrigation: a) Schematic of low atmospheric winds (same as Fig. 2 in the main text); Monthly mean irrigation donations (grid box average) from Irrigation simulation IRRmin: b) March, c) April, d) May, e) June, f) July, g) August

Figure S2.

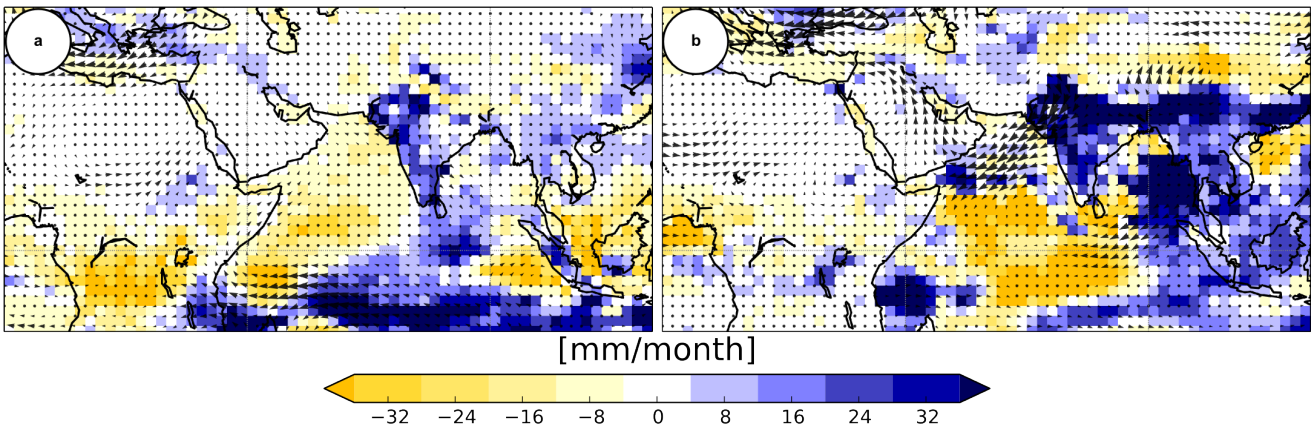

Supporting Material Fig. 3: Impact of irrigation on the upward moisture flux (evapotranspiration - precipitation) and the low level wind field (1000 - 600 hpa): Difference in upward moisture flux between IRRmin - REF: a) March, b) May; black arrows and dots indicate differences in the low level wind field.

Several mechanisms can be identified, by which the changes in the upward moisture flux and the wind field enhance the effects of the increased advective moisture transport towards remote regions.

a) (March) In the northern part of the Arabian Sea the upward moisture flux is negative, confirming that the moisture advected towards the Horn of Africa does not originate from an increase in evaporation over the ocean. On the contrary, the air becomes dryer while it is advected accross the Arabian Sea. East of the coast of Tanzania, there is an increase in the speed of the easterly winds, while the windspeed of the easterly winds south of the Bay of Guinea decreases. Therefore, more humidity is transported towards Africa from the east and less moisture is advected away from Africa's west coast, which enhances the moisture convergence in the region south of the Congo.

b) (May) The westerly winds in the northern part of the Arabian Sea are weaker in IRRmin. Hence, less moisture is advected eastwards from the Arabian Peninsula and the Horn of Africa. Also the easterly winds in the Gulf of Guinea are slightly weaker, so that less water vapor is transported offshore, away from the west coast of Africa.

Figure S3.

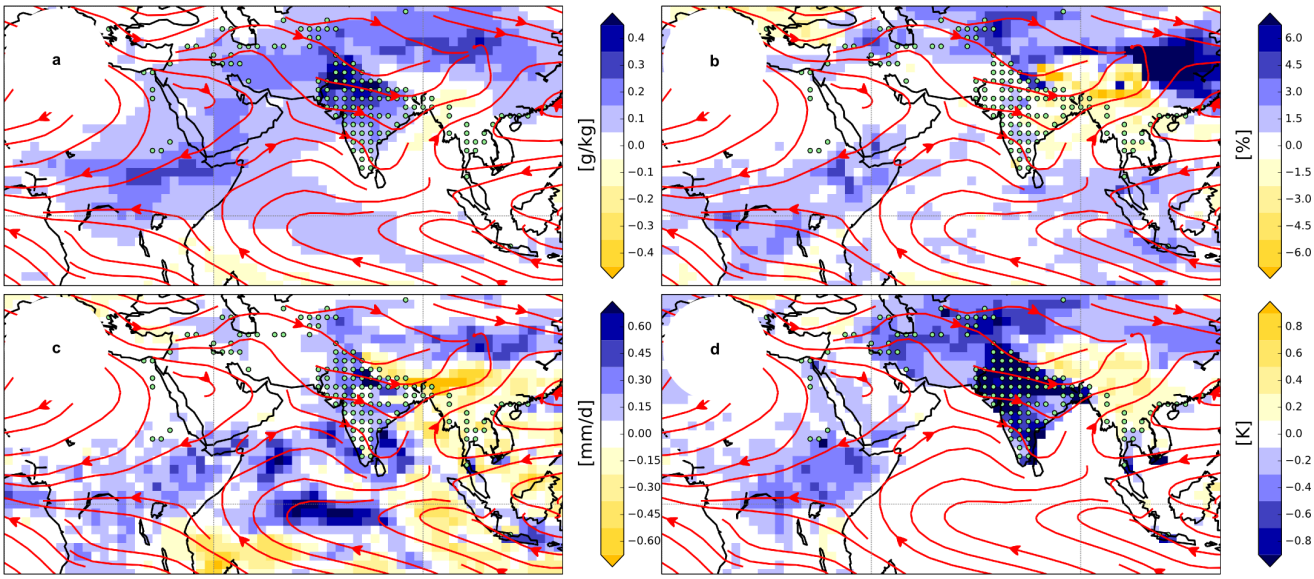

Supporting Material Fig. 4: Connection of atmospheric water vapor, cloud cover, precipitation and surface temperatures: 20-year annual mean difference (IRRmin - REF) of: a) specific humidity and b) cloud cover in the low atmosphere (1000 - 600 hpa), c) precipitation and d) surface temperature; red streamlines indicate wind directions from the irrigation run, dotted areas indicate grid box mean irrigation > 40 mm / a

Figure S4.

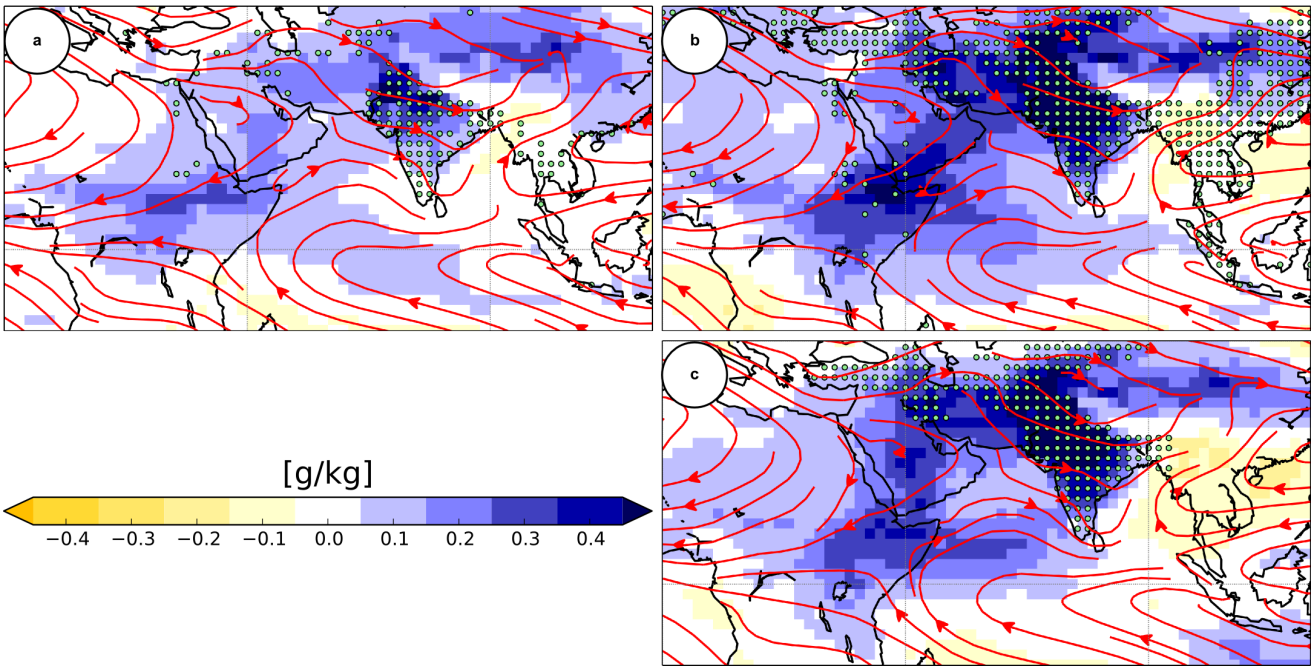

Supporting Material Fig. 5: Atmospheric water vapor in different irrigation scenarios: 20-year annual mean difference in specific humidity in the low atmosphere (1000 - 600 hpa): a) IRRmin - REF, b) IRRmax - REF, c) IRRideal - REF; red streamlines indicate wind directions in the low atmosphere (1000 - 600 hpa) of the irrigation run, dotted areas indicate grid box mean irrigation > 40 mm / a

IRRideal : Idealized irrigation simulation similar to IRRmax , in which irrigation was limited to an area in Asia between 30° E - 95° E, excluding the Arabian Peninsula. The simulation was used to confirm that impacts in remote regions are related to water vapor advected from regions in the Middle East and South Asia, and not the result of local irrigation. Comparing subfigures b and c shows that for IRRideal the simulated impact on the specific humidity in the lower atmosphere is similar to IRRmax. Consequently, even with irrigation limited to the area described above, there is still a pronounced increase in the advective moisture transport into Africa and towards the east coast of China. With robust increases in precipitation around the African Great Lakes, this places the closest irrigated areas in Iran and Iraq in a distance of at least 4000 km (not shown). From regions at China's east coast, with relative precipitation increases of 15 %, the distance to the nearest irrigated area is well above 2500 km (not shown).

Figure S5.